PHYSICAL REVIEW B **89**, 045428 (2014)

Using high pressure to unravel the mechanism of visible emission in amorphous Si/SiO_x nanoparticles

A. R. Goñi,[1,2] L. R. Muniz,[2] J. S. Reparaz,[2] M. I. Alonso,[2] M. Garriga,[2] A. F. Lopeandia,[3] J. Rodríguez-Viejo,[3,4] J. Arbiol,[1,2] and R. Rurali[2]

[1]*ICREA, Passeig Lluís Companys 23, 08010 Barcelona, Spain*

[2]*Institut de Ciència de Materials de Barcelona (ICMAB-CSIC), Campus UAB, 08193 Bellaterra, Spain*

[3]*Dept. de Física, Universitat Autònoma de Barcelona, 08193 Bellaterra, Spain*

[4]*MATGAS Research Centre, Campus UAB, 08193 Bellaterra, Spain*

(Received 31 October 2013; revised manuscript received 24 December 2013; published 28 January 2014)

Regarding light absorption/emission efficiency, silicon presents the fundamental drawback of its indirect band gap. It is long known, though, that optical properties are greatly enhanced in materials which comprise different kinds of nanocrystalline Si covered by or embedded in Si oxide layers. Conversely, their amorphous counterparts have received far less attention, such that no general consensus about the emission mechanism prevails. We report here on an efficiently luminescent material based on amorphous Si nanoparticles (a-Si NPs) embedded in a nonstoichiometric Si oxide matrix, which exhibits intense, broadband emission from the a-Si NPs, spectrally separable from the defect luminescence of the suboxide matrix. Apart from the brightness of the emitted light, the nanometer-size a-Si inclusions present the technological advantage of needing very moderate annealing temperatures (450 °C–700 °C) for their production. The combined use of high pressure, experimentally as well as theoretically, allowed us to trace back the microscopic origin of the photoluminescence to radiative recombination processes between confined states of the a-Si NPs. The signature of quantum confinement is found in the magnitude and sign of the pressure coefficient of different optical transition energies. The pressure derivatives exhibit a universal dependence on particle size, determined solely by the confinement energy of the discrete electron state involved in the radiative recombination process.

DOI: 10.1103/PhysRevB.89.045428 PACS number(s): 62.50.−p, 78.67.Hc, 07.35.+k

I. INTRODUCTION

The scientific community is well aware of the technological/economical importance of finding materials which are efficient light emitters and, simultaneously, fully compatible with nowadays silicon-based microelectronics. Problems of integration and the need of complicated chip architectures are continuously jeopardizing the development of optical interconnects in information technology due to the lack of a bright light source made of Si, Ge, and/or their alloys. The fundamental reason is the indirect nature of their band gap and the consequent detriment by about five orders of magnitude in the probability of emitting or absorbing photons at those energies. In this respect, the about simultaneous discovery of bright, broadband visible luminescence at room temperature from porous silicon [1] and colloidal oxidized Si nanocrystals [2] constituted real breakthroughs that triggered intense and widespread activity in the field, lasting until today. Thereafter, it followed a frantic quest for all kinds of light-emitting materials based on oxidized/nanocrystalline silicon heterostructures synthesized by a great variety of techniques [3]. Another milestone in the development of photonic devices based on Si was the achievement of lasing action in optically pumped Si nanocrystals dispersed in a silicon dioxide matrix [4]. Since then, the emerging field of silicon photonics has evolved into technological reality (see Ref. [5] for an extensive review).

From the very beginning, the origin of the bright visible luminescence of porous silicon as well as of crystalline Si nanoparticles (c-Si NPs) was a matter of intense debate. Quantum confinement effects were immediately invoked as an essential aspect of the mechanism for radiative recombination in this class of materials [1,6–8]. The most relevant pieces of information in favor of confinement effects are the blue-shift with decreasing nanoparticle (NP) size of the photoluminescence (PL) band [9–14] and/or the optical absorption edge [9,15,16] and the variation of the PL peak position with temperature [17,18]. However, the similarity of the emission spectra of different kinds of nanocrystalline Si/Si oxide materials, the influence of the atmosphere on the PL intensity (aging in air or hydrogen passivation) and/or strong illumination upon it, or the observation of very large Stokes shifts between absorption and emission, led many researchers to the conclusion that this visible emission might originate from recombination in the oxide matrix [19–22]. The nonbridging oxygen-hole defect (Si==O) at the interface between the c-Si NP and the oxide matrix was proposed as the most likely recombination center [23]. It slowly became clear that part of the emission spectrum exhibits indeed contributions from interfacial defects [14,17,24–29]. To reconcile the sometimes contradictory experimental evidence favoring one or the other possibility, Qin and Li proposed the quantum-confinement/luminescent-center model [30]. The main idea here is that the photoexcitation of electron-hole pairs occurs always in the Si nanocrystals, whereas for the photoemission there are two competing processes: the recombination between quantum confined states of the c-Si NPs and the recombination at luminescent defect centers in the adjacent Si oxide. Which is the dominant process would be determined by the carrier capture cross section, emission efficiency, defect density, and size of the NPs. Later, a refinement of this model seemed to indicate that the main PL arises from optical transitions

 ©2014 American Physical Society

between interface defect states close to the conduction band edge of the Si NP and midgap defect levels of the Si oxide with energies close to the top of the Si valence band [31]. For a detailed retrospective on this topic, we refer to the review of Qin *et al*. [32]. The report of an ultrafast (picosecond range) visible band in the PL spectrum of Si nanocrystals installed again quantum confinement in the focus of the debate, for this emission is assigned to direct optical transitions between higher-lying confined levels of the Si nanocrystals [33].

In comparison, reports on the optical emission properties of amorphous Si (a-Si) nanostructures are really scarce in the literature. Visible light emission at room temperature from oxidized, hydrogenated a-Si was reported by Bustarret *et al*. early in 1992 [34]. Subsequently, photoluminescence emission in the visible spectral range was obtained from a-Si/SiO_2 superlattices with Si layer thicknesses between 1 and 3 nm [35]. Interestingly, the PL peak energies displayed an inverse proportionality with a-Si layer thickness, a fact taken as evidence of quantum confinement effects in the amorphous films. Almost simultaneously, the absorption edge spectrum of very thin a-Si films sandwiched between amorphous silicon nitride layers also exhibited a blue-shift with decreasing layer thickness and the extracted density-of-states (DOS) resembled the staircaselike DOS of quantum wells [36]. Porous silicon produced from hydrogenated amorphous Si was also shown to be strongly luminescent [37]. The study of confinement effects by analyzing the PL spectra *in situ* during anodization in hydrofluoric acid yielded an intriguing result [38]: no blue-shift of the PL peak maximum was observed when carrying out the experiment with amorphous silicon, as compared to crystalline porous Si. This was interpreted as due to disorder which should lead to a strong localization of the electron wave function within about 1 nm. Nevertheless, a few years later, Park *et al*. [39] decided to take advantage of the higher PL efficiency of a-Si to produce a-Si NPs embedded in silicon nitride. It was clearly shown that for particle diameters between 1.5 and 2.5 nm, both the PL peak energy as well as the optical absorption energy shifted with NP size according to the expectations from effective mass theory.

First theoretical efforts tackled the dependence of the main (optical) gap on the size L of nanocrystalline Si clusters. The standard density-functional approach (DFT) yielded for c-Si NPs a gap scaling as L^{-1} [40], the dependence of which was subsequently taken as bold evidence for confinement effects [9,12,27,41,42]. Optical transitions at the gap were also reported to become increasingly dipole allowed with the reduction of L below a few nanometers. The same behavior of the gap was extracted for crystalline porous Si using the technique of linear combination of atomic orbitals, applied to quantum crystallites and wires with varying diameter [43]. Later, quasiparticle gaps including self-energy corrections and also accounting for exciton Coulomb energies were calculated using the pseudopotential method [44]. Precision was improved in the calculations by adequate treatment of the exchange interaction using time-dependent DFT [45], bridging experimental and theoretical results. The application of first-principles calculations, though, is usually limited to crystal sizes below 4 nm (about 1000 atoms) due to the computational cost. Thus, semiempirical methods within the envelope function approximation (EFA) such as $k \cdot p$ were used to study the electronic and optical properties of larger single c-Si NPs and their ensembles, including the conditions for stimulated emission [46]. As far as the optical matrix elements are concerned, the most exhaustive work considered electron-hole exchange interactions that lead to exciton formation, accounting for symmetry considerations [47]. In contrast, for amorphous Si nanostructures, the localized nature of the band-tails states poses an additional difficulty when considering confinement effects. The first modeling attempt [48] considered that the electronic states as well as the radiative recombination processes were those of *bulk* a-Si [49] but imposing the geometrical restriction given by the size of a given nanostructure. Just by statistics, the number of accessible localized and deep defect states decreases with decreasing nanostructure size, leading to an effective increase in the optical emission and radiative recombination rate, respectively. A further refined model that took into account the changes in electronic structure for the amorphous phase of Si by means of empirical tight-binding calculations [50] yielded the following picture: Delocalized states experience the full confinement effect as for c-Si, whereas strongly localized states with energies deep in the gap are completely insensitive to confinement. Weakly localized states of the band tails exhibit a similar but intermediate blue-shift as compared to the crystalline counterparts. More recently, calculations also using the tight-binding method with a larger atomic orbital basis and, more importantly, a realistic structure model for the amorphous phase [51] were able to reproduce extremely well the size dependence of the emission peak energy measured for a-Si NPs with diameters between 1.4 and 2.5 nm [39]. A much larger radiative recombination rate for a-Si NPs as compared to c-Si ones was also obtained and explained as due to disorder-induced effects.

The application of high hydrostatic pressure has proved to be a powerful tool for gaining insight into the electronic and optical properties of semiconductor nanostructures since it allows for a controlled reduction of interatomic distances and a continuous modification of the energy states. A key element is that tetrahedrally coordinated semiconductors such as the group-IV materials Si and Ge, as well as all III-V and II-VI compounds, exhibit a clear systematics regarding the pressure dependence of the fundamental band gaps [52]. The direct gap at the Brillouin-zone center shifts up with increasing pressure at a typical rate of 100 meV/GPa, whereas the indirect gap between the X point of the conduction band and the top of the valence band at zone center displays a negative but much smaller pressure coefficient of approximately -10 meV/GPa. In this way, just by measuring the pressure coefficient of an optical transition, it is possible to pinpoint its origin in relation to the band states of the bulk material. Cheong *et al.* pioneered the use of high hydrostatic pressure to study porous silicon [53] and Si nanocrystals embedded in SiO_2 [54]. In both cases, a slightly negative pressure coefficient is obtained for the shift of the PL maximum, which is of the same order of magnitude but smaller than the one measured in bulk Si [55]. Unfortunately, the authors interpreted their experimental results as speaking against quantum confinement, mainly misled by the use of an oversimplified particle-in-a-cubic-box model. In contrast, a very recent report of a negative pressure dependence of the center of mass of the visible emission band from colloidal Si NPs was indeed taken as evidence that the efficient PL arises from

quantum confined states [56]. Although the measured pressure coefficients are larger in magnitude than for bulk Si, result which is difficult to understand for NPs with diameters of 2.6 to 4.6 nm, we fully comply with this interpretation. The aim of our work is to make explicit use of the mentioned systematics in the band-gap pressure coefficients to unravel the microscopic origin of radiative recombination in *amorphous* Si NPs.

In this paper, we present a systematic study of the pressure dependence of the visible emission of several samples containing a-Si NPs with different average diameters embedded in a Si suboxide matrix. By careful analysis of the PL line shapes in terms of a set of Gaussian functions tentatively attributed to inhomogeneously broadened optical transitions between confined states of the a-Si NPs, we were able to determine the pressure derivatives of the peak energies with sufficient accuracy to unravel a systematic trend of the pressure coefficients as a function of particle size and transition energy. The observed trends are corroborated by first-principles electronic-structure calculations. Although they are performed for nanocrystals of 1 to 4 nm in diameter, we give plausibility arguments that the outcome of the theory is also representative for amorphous nanometer-size inclusions.

II. EXPERIMENT

The Si nanoparticle (NP) samples were prepared following a simple, technologically friendly two-step procedure which is fully compatible with nowadays complementary metal-oxide semiconductor (CMOS) fabrication. First, nonstoichiometric silicon oxide layers with thicknesses between 200 and 300 nm were deposited by electron beam evaporation on Ge(001), Si(001), or glass substrates using a SiO target of 99.9% purity from CERAC. During growth the oxygen partial pressure was kept at 4×10^{-5} mbar to minimize on-flight oxidation of the Si atoms, which guarantees the growth of suboxides with a typical composition of $SiO_{1.2}$, i.e., low-oxygen content. The resulting layers are amorphous and very porous. The growth rate was fixed at 0.5 nm/s with the aid of a calibrated quartz crystal monitor located near the substrates. Subsequently, the as-grown layers were annealed inside the furnace of a differential scanning calorimeter, Perkin-Elmer Series 7, at very moderate temperatures ranging from 450 °C to 700 °C under Ar atmosphere. The as-grown films were ramped up in temperature at a rate of 50 °C/min until the desired temperature, isothermally annealed for 1 h and cooled down to ambient at 100 °C/min.

Energy-filtered transmission electron microscopy (EFTEM) measurements were carried out using a field-emission 200-keV Jeol 2010F microscope equipped with a Gatan dodecapole-based electron image filter (GIF 2000), which adds the capability of performing electron energy-loss spectroscopy. In order to enhance the image contrast between pure Si and silicon suboxide, the TEM images were energetically filtered at around 17 eV, the energy of the Si plasmon, which is sufficiently separated from the SiO_2 plasmon placed at 22 eV [57,58]. For all EFTEM measurements, the slit width was kept at 2 eV. Samples for TEM observation were prepared as cross sections, first grinded and finally ion milled.

Fourier-transform infrared (FTIR) measurements were performed in reflectivity configuration using a Fourier-transform infrared Bruker Vertex-70 system equipped with an accessory to automatically vary the angle of incidence. Reflected light intensity was measured with a liquid-N_2 cooled mid-band HgCdTe detector in the spectral range from 570 to 4000 cm^{-1}. A reference spectrum was taken at an angle of incidence of 15°. FTIR measurements were conducted without polarizer at 50° of incidence, normalizing the reflected intensity by that of the reference spectrum.

The high-pressure photoluminescence measurements were performed at room temperature employing a gasketed diamond anvil cell (DAC). The sample was thinned from the substrate side to about 30 μm by mechanical polishing and placed into the DAC together with a ruby sphere for pressure calibration [59]. A 4:1 methanol/ethanol mixture was used as pressure-transmitting medium for best hydrostatic conditions up to 10 GPa. Helium was also used in one case for comparison. The PL spectra of the sample were excited using the 405-nm line of a solid-state laser and collected using a LabRam HR800 spectrometer equipped with a charge-coupled device detector. PL spectra were corrected for the spectral response of the spectrometer by normalizing each spectrum using the detector and grating characteristics. The incident light power density was about 60 W/cm^2.

III. RESULTS AND DISCUSSION

A. Characterization of the a-Si nanoparticles embedded in $SiO_{1+\delta}$

The samples under study consist of fairly spherical silicon inclusions with average diameters between 1.5 and 2.5 nm embedded in a Si-suboxide matrix. After deposition of the suboxide layer on a substrate, the Si NPs form during thermal annealing at very moderate temperatures between 450 °C and 700 °C, as compared to the usual annealing step carried out above 1000 °C, which is necessary to obtain crystalline inclusions [4,8,11,13,14,17,18,21,28,29,54]. The low annealing temperatures, in turn, seem to lead to noncrystalline particles since we are unable to find any evidence of crystallinity in Raman as well as electron diffraction spectra. The Si NPs form by thermally activated phase separation [60]:

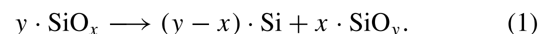

$$y \cdot SiO_x \longrightarrow (y-x) \cdot Si + x \cdot SiO_y. \quad (1)$$

In this way, the average particle size and the suboxide matrix stoichiometry are controlled by the annealing temperature. The mild thermal annealing produces highly porous SiO_x matrices with a relatively low oxygen content of $x = 1.2$–1.8. Hence, at ambient conditions, molecular oxygen is always present inside the suboxide matrix, which has important consequences for the optical emission.

Energy-filtered transmission electron microscopy (EFTEM) images nicely confirm the presence of Si NPs embedded in the silicon oxide matrix, as shown in the cross-section micrographs of Figs. 1(a) and 1(b) for a sample annealed at 550 °C and 700 °C, respectively. In these images, pure Si corresponding to the NPs as well as the Si substrate is visualized as bright regions, whereas the SiO_2 matrix appears dark. In fact, to enhance the contrast between both materials, the shown EFTEM images correspond to the

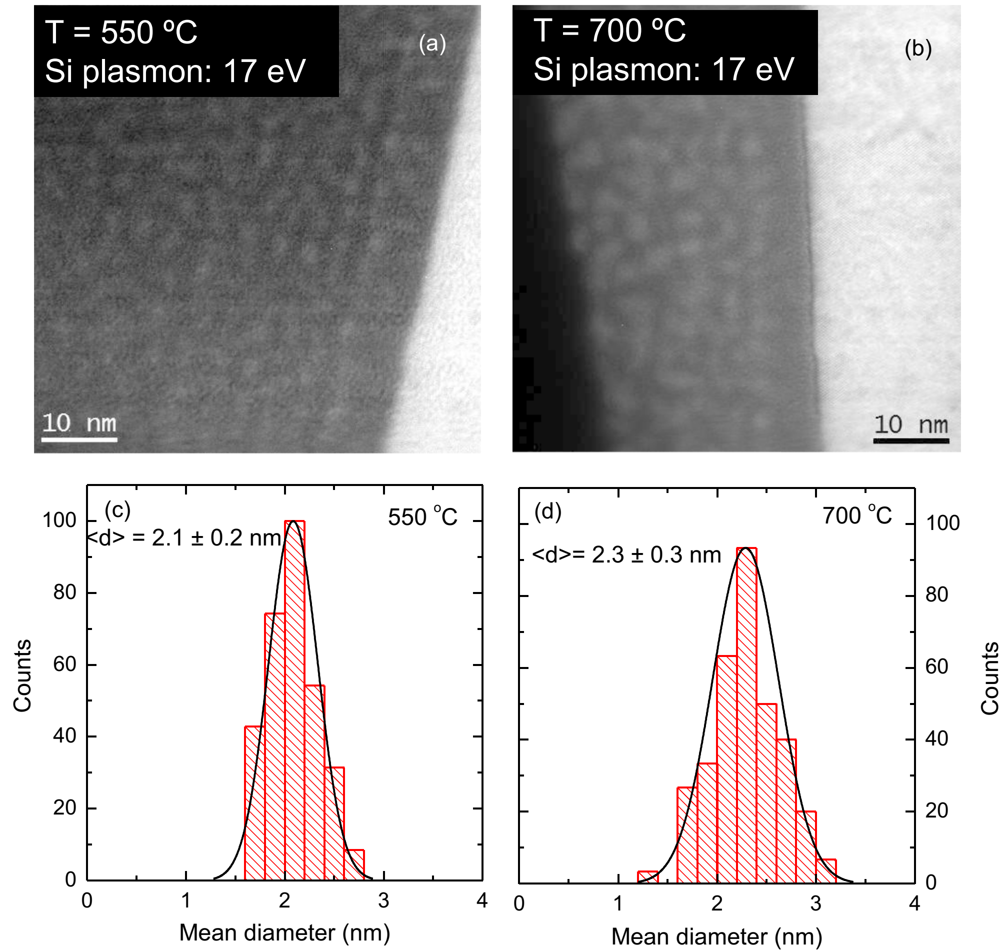

FIG. 1. (Color online) (a) Energy-filtered TEM micrographs of the sample annealed at 550 °C clearly showing the presence of Si NPs embedded in the suboxide matrix. The Si NPs and the Si substrate appear bright, whereas the dark regions correspond to suboxide material. (b) Idem (a) but for the sample annealed at 700 °C. (c) Particle-size histogram of the sample annealed at 550 °C constructed by sampling more than 300 NPs. The resulting size distribution is fairly sharp with a mean diameter of (2.1 ± 0.2) nm. (d) Idem (c) but for the sample annealed at 700 °C. The mean diameter of (2.3 ± 0.3) nm is only slightly larger.

composition of two images obtained by centering the electron filter either at the energy of the bulk Si plasmon or at that of the SiO_2 plasmon [57,58]. In addition to the EFTEM measurements, electron diffraction patterns were obtained from selected areas on the SiO_2 layers. The patterns did not show any dotted diffraction rings compatible with the presence of randomly oriented crystalline NPs. In fact, the patterns looked like a unique wide diffused ring, as is typical for an amorphous material. This means that the Si NPs most likely have a disordered nature. Statistical analysis of the complete EFTEM images over a population of more than 300 NPs yielded the size histograms depicted in Figs. 1(c) and 1(d). In order to minimize the heating effects caused by the electron beam, the images used to construct the histograms were obtained with the lowest possible exposure times. The resulting size distributions are fairly narrow, exhibiting an average diameter of 2.1 ± 0.2 nm and 2.3 ± 0.3 nm for the sample annealed at 550 °C and 700 °C, respectively. As shown in the following, such a small difference in mean particle size is fully compatible with the results of infrared vibrational spectroscopy and is enough to substantially influence the optical emission spectra of the Si NPs.

Before discussing the optical emission, it is instructive to analyze the data from Fourier-transform infrared (FTIR) vibrational spectroscopy, for it yields valuable information about the composition of the suboxide matrix and its changes after each annealing step as well as about the gradual formation of the Si NPs themselves. In FTIR, special attention was paid to the asymmetric Si-O-Si stretching vibration of oxygen atoms in twofold-coordinated bridging bonding sites centered at around 1000 cm^{-1}, for which there exists a calibration of the integrated absorption as a function of the oxygen concentration of the suboxide matrix [61,62]. The absorption coefficient α is obtained as

$$\alpha(\omega) = -\frac{1}{t} \ln\left(\frac{1 - R(\omega)}{1 - R_0(\omega)}\right), \qquad (2)$$

where $t = 200$ nm is the suboxide layer thickness and $R(\omega)$ and $R_0(\omega)$ are the light intensities measured in reflectivity at 50° and 15°, respectively, at photon frequencies ω in the vicinity of the Si-O-Si stretching band. The integrated absorption is then a direct measure of the amount of twofold-coordinated oxygen bound to silicon and present in the SiO_x layer, from which its composition is obtained following the

procedure developed for studying hydrogenated amorphous silicon and germanium [61]:

$$\rho^{O}_{\text{atoms}}(\text{cm}^{-3}) = A_{\text{stretch}} \int_{\omega_{\text{stretch}}} \frac{\alpha(\omega)}{\omega} d\omega, \quad (3)$$

where ρ^{O}_{atoms} is the oxygen concentration, i.e., number of O atoms per cm^{-3} pertaining to the SiO_2 phase, and $A_{\text{stretch}} = 1.6 \times 10^{18}$ cm^{-2} is the calibration constant determined for Si-O-Si stretching vibrations in silicon dioxide [62].

Figure 2(a) shows the absorption coefficient at infrared frequencies of the Si-O-Si stretching vibrations measured on the as-grown sample and four pieces of it, annealed at different temperatures between 450 °C and 700 °C. From the integrated intensity of such absorption bands [Eqs. (2) and (3)] we obtained, in the case of the as-grown SiO_x layers, a fairly low composition of $x \approx 1.2$. Thermal annealing promotes phase separation of the nonstoichiometric suboxide into the two thermodynamically stable phases: a pure Si phase (in amorphous or crystalline form), seeding at Si-rich regions, and an amorphous silica phase. In fact, the strong increase in integrated absorption of the Si-O-Si stretching band due to thermal annealing, as seen in Fig. 2 (a), is a clear indication of the incremental amount of twofold-coordinated oxygen present in the suboxide layer. The resulting compositions are plotted in Fig. 2(b) as a function of annealing temperature. Even at 700 °C the suboxide is not completely stoichiometric, having a composition of $x \approx 1.8$. Obviously, the amount of pure silicon (amorphous or crystalline) increases during annealing as well. Using Eq. (1), we can infer the average number per cm^{-3} of Si atoms in the elemental phase and the

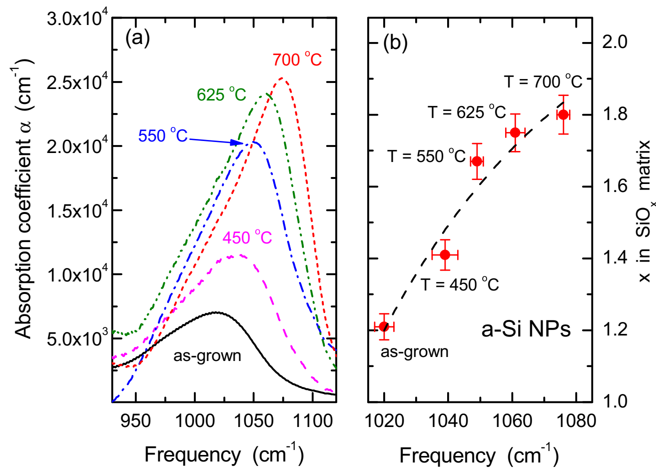

FIG. 2. (Color online) (a) Fourier-transform infrared (FTIR) absorption spectra of the as-grown silicon oxide layer and four different pieces annealed at 450 °C, 550 °C, 625 °C, and 700 °C in the frequency region of the asymmetric Si-O-Si stretching vibration of oxygen atoms in twofold-coordinated bridging bonding sites. The integrated intensity of this absorption band is used to monitor the changes in composition of the suboxide upon annealing. (b) The oxygen content of the SiO_x matrix as determined by FTIR for the five studied samples. Thermal annealing triggers phase separation processes in the suboxide matrix, leading to an increasingly stoichiometric matrix material and the further formation of pure Si NPs, as the annealing temperature increases.

TABLE I. Results of the analysis of the infrared data for samples annealed at different temperatures T_{ann}, where $(y - x)$ is the change in composition of the suboxide, $\rho^{\text{Si}}_{\text{atoms}}$ and $\rho^{\text{Si}}_{\text{NPs}}$ are the density of Si atoms in the elemental phase and of Si NPs, respectively, and d the average NP diameter. Diameter values in boldface correspond to experimental ones determined by EFTEM for the samples annealed at 550 °C and 700 °C. Numbers in parentheses represent error bars.

T_{ann} (°C)	$(y - x)$	$\rho^{\text{Si}}_{\text{atoms}}$ (cm^{-3})	$\rho^{\text{Si}}_{\text{NPs}}$ (cm^{-3})	d (nm)
450	0.20(5)	$1.0(2)\times10^{22}$	$9.5(3)\times10^{19}$	1.6
550	0.46(5)	$2.3(2)\times10^{22}$	$9.5(3)\times10^{19}$	**2.1**(0.2)
625	0.54(5)	$2.7(2)\times10^{22}$	$9.6(3)\times10^{19}$	2.2
700	0.60(5)	$3.0(2)\times10^{22}$	$9.4(3)\times10^{19}$	**2.3**(0.3)

density of Si NPs, respectively, as given by

$$\rho^{\text{Si}}_{\text{atoms}}(\text{cm}^{-3}) = (y - x) \cdot \frac{\rho_{\text{Si}}}{m_{\text{Si}}}, \qquad \rho^{\text{Si}}_{\text{NPs}}(\text{cm}^{-3}) = (y - x) \cdot \frac{6}{\pi d^3}, \quad (4)$$

where $\rho_{\text{Si}}/m_{\text{Si}} \sim 5.0 \times 10^{22}$ cm^{-3} is the ratio of the bulk Si density over its atomic mass and d is the average NP diameter. The calculated values of $\rho^{\text{Si}}_{\text{atoms}}$ and $\rho^{\text{Si}}_{\text{NPs}}$ together with the changes in composition of the suboxide matrix determined by FTIR spectroscopy are listed in Table I for the different annealing temperatures. The highlighted diameters correspond to the values determined by EFTEM for the samples annealed at 550 °C and 700 °C. Since the NP density appears to remain essentially constant upon annealing, for the two samples lacking EFTEM data, we have calculated the diameter compatible with that NP density. The quantitative agreement between the EFTEM and FTIR results shown in Table I is remarkable. The conclusion of this analysis is that the $SiO_{1.2}$ as-grown layer presents a high density of seeding points of about 1×10^{20} cm^{-3}. Upon annealing, the Si particles grow in size but not in number, reaching average diameters between 1.6 and 2.3 nm and being closely packed within the suboxide matrix. The latter might have important implications for device applications.

B. Emission properties at ambient pressure

Figure 3(a) shows representative room-temperature PL spectra of an as-grown layer and four pieces annealed at different temperatures excited with the 405-nm line using a low-power density of about 60 W/cm^2. Whereas the as-grown sample exhibits almost no emission except for a faint band centered at about 2.35 eV, the samples containing Si NPs show an intense and broadband PL, extending from the near infrared to the green part of the visible spectrum. Since the average Si NP size also increases with increasing annealing temperature, the monotonous red-shift of the whole emission band observed in the spectra of Fig. 3(a) is a signature of quantum confinement. Strikingly, the emission efficiency and spectral characteristics of the disordered (amorphous) Si NPs are totally similar to the ones exhibited by their crystalline counterparts of the literature. We thus confirm previous results [34,39], indicating that crystallinity is not essential for attaining intense and broadband light emission. Within

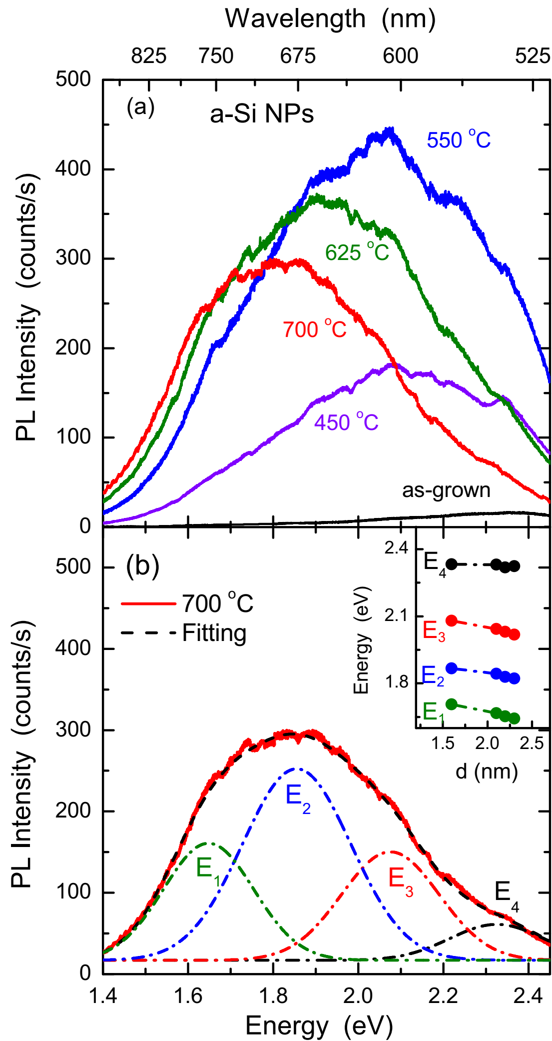

FIG. 3. (Color online) (a) The red-shift of the whole PL band with increasing annealing temperature, i.e., for larger Si NP diameters, is a clear indication that quantum confinement effects are at work. The extremely faint emission from the as-grown layer is associated with luminescence from defect centers in the suboxide matrix. (b) An example of the line-shape fitting analysis of the PL spectra performed with four Gaussian peaks labeled $E_1,\ldots,E_4$. The three lowest-energy peaks, which can be assigned to optical transitions between different confined states of the a-Si NPs, exhibit similar red-shifts upon annealing, i.e., with increasing average NP diameter d, as displayed in the inset.

the quantum confinement model, the emission spectrum of an ensemble of Si NPs is expected to consist of a superposition of inhomogeneously broadened Gaussian peaks. The incipient peaklike structure exhibited by the measured PL spectra complies with this idea, although large widths prevent from resolving individual peaks. Figure 3(b) shows, for example, the line-shape analysis performed with four Gaussians in the case of the sample annealed at 700 °C. Starting with the lowest-energy peak, each one is labeled as E_i with $i = 1,2,\ldots$, corresponding to the principal quantum number due to confinement. We emphasize that four is the minimum number of Gaussians that allows for a very satisfactory description of the PL line shape [dashed red line in Fig. 3(b)] and its changes with temperature and upon the application of external pressure for all Si NP samples. This can not be achieved with one less Gaussian and, in turn, one additional peak is simply redundant. As demonstrated further below, the weak PL band observed for the as-grown sample in the energy range between 2.2 and 2.4 eV, approximately, corresponds to the optical emission associated with luminescent defect centers of the silicon oxide matrix. Since the E_4 peak totally overlaps with the defect PL, for a discussion of pressure/temperature effects on the Si NP luminescence, we will restrict ourselves to the three remaining peaks at lower energies.

We note that, whereas the description of the broad emission band using several overlapping peaks is just a heuristic fact that results from the careful analysis of the changes of the PL spectra upon variation of pressure, temperature, or particle size, their interpretation is not obvious. As mildly anticipated in the previous paragraph, we would like to put forward an interpretation based on radiative recombination processes between quantum confined states of the a-Si NPs (ground as well as excited states). We intend to subsequently consolidate such underlying physical model of light emission by providing experimental as well as theoretical evidence. For that purpose, we start by digressing briefly on PL linewidths. The full widths at half maximum (FWHM) of the whole PL band in our four samples at ambient conditions are roughly 780, 760, 660, and 560 meV for the samples annealed at 450 °C, 550 °C, 625 °C, and 700 °C, respectively. These widths are unexpectedly large, being typically 1.5 to 2.5 times that of the PL linewidths reported for c-Si NPs throughout the literature [10,12,13,15,17,27,28,31,56]. In contrast, the FWHM of the PL spectrum reported by Park *et al.* [39] for a-Si NPs with mean diameter of 1.9 nm is ca. 640 meV, similar to that measured in our particles of 2.1 nm in diameter (see Table I). In the following, we show that such large linewidths can not be explained by band-gap fluctuations due to the size distribution of the NP ensemble for the values of mean diameter and variance determined for our samples. For a system of CdSe quantum dots embedded in a quaternary matrix it has been demonstrated that when inhomogeneous broadening is at work, the linewidth and energy position of the PL peak corresponding to the ground-state emission follow the relation [63] $\Gamma \propto \Delta d(E_{\mathrm{PL}} - E_{\mathrm{gap}})^{3/2}$. In our case, $\Delta d = 0.3$ nm is the NP diameter variation from TEM and $E_{\mathrm{gap}} = 1.1$ eV is the band-gap energy of bulk Si. Since within this very crude approximation Γ depends on the confinement energy $E_{\mathrm{PL}} - E_{\mathrm{gap}}$, we have generalized this equation to account also for the excited emission peaks of the same NP ensemble. In this way, we predict a gradual increase in peak width with increasing emission energy. Empirically, the widths were determined such as to yield the best fits to the PL spectra measured at ambient pressure and temperature conditions. For the sample annealed at 550 °C, for example, the first three widths read as 190(160), 280(250), and 340(350) meV, where the numbers in parentheses correspond to the calculated values using the simple equation mentioned above. The quantitative agreement is surprisingly good, providing further support to the interpretation of the Gaussian peaks in terms of PL emission from confined states. Furthermore, the rough estimates are also in good agreement with the resulting linewidths obtained using more refined calculation

methods for NP ensembles with similar size-distribution functions [46,64].

A problem with the proposed interpretation is that it implies the observation of strong luminescence from higher excited states under continuous-wave (cw) illumination, which is *usually* extremely weak due to the fast nonradiative hot-carrier relaxation. We believe that the a-Si NPs constitute a peculiar system which appears to fulfill the necessary conditions for the observation of the phonon bottleneck effect. Since its prediction [65], this effect remained controversial and lacked of convincing experimental evidence. A phonon bottleneck should manifest itself in a dramatic decrease in the main energy-relaxation channel via electron-phonon interaction, originating from a mismatch between the vibrational spectrum and that of well-separated discrete electronic levels in systems dominated by quantum confinement effects. In particular, when the interlevel spacing becomes larger than the cutoff optical phonon frequency, energy relaxation of hot carriers due to *single*-phonon emission should be widely suppressed (note that higher-order multiphonon processes, characterized by a much lower relaxation rate, are not affected by the bottleneck) [66]. In our a-Si NPs, the energy difference between consecutive optical transitions represented by the fitted Gaussians are ca. 200 meV. If the hole states are more closely spaced in energy than those of electrons, although this is not a necessary condition, the separation between confined conduction-band levels is much larger than the highest optical phonon energy of about 55 meV (note that phonons soften in the amorphous as compared to the crystalline material). Thus, the phonon bottleneck should slow down phonon-assisted relaxation into the lowest-energy levels E_1 and E_2, whereas the relaxation between higher-energy levels above E_3 proceeds as usually fast. In fact, a slowing down by about three orders of magnitude in the relaxation rates of excited levels was already observed in pretty small CdSe colloidal quantum dots and ascribed to buildup of a phonon bottleneck [67].

There are, however, other relaxation pathways competing with the phonon bottleneck effect, such that relaxation to the ground and first excited states still occurs, making possible the radiative emission from the lowest-energy states despite the bottleneck. Intraband Auger relaxation can be completely ruled out in our case due to the very low-excitation powers used, for which it is almost impossible to have more than one electron-hole pair simultaneously at the same NP. Interband Auger processes, in contrast, are extremely fast, but rather than leading to an energy relaxation such energy exchange between electrons and holes effectively produces a nonthermal population of the discrete levels [66]. Structural and surface defects can further lead to a partial lifting of the degeneracy of the discrete levels of a crystal with the concomitant creation of a dense distribution of energy states [68]. This effect, which should be enhanced in amorphous particles due to their disordered nature, is widely counteracted by strong carrier confinement to nanometer-sized particles, as shown elsewhere [50,51]. In addition, it has been recently rationalized that the phonon bottleneck is reinforced by pure dephasing (decoherence) caused by *elastic* electron-phonon scattering [69]. For this to happen, phonon-induced dephasing times in the 10-fs range are required, much faster than the time scale of the coherent inelastic electronic transition between two discrete states. Dephasing rates should further increase in disordered particles due to electronic potential fluctuations. Hence, one can speculate that due to the combined effect of quantum decoherence and phonon bottleneck, the net nonradiative relaxation is sufficiently slowed down such that radiative recombination of hot carriers in excited states gives rise to an important contribution to the emission spectrum of a-Si NPs. For sure, this assumption ought to be confirmed by direct measurements of nonradiative versus radiative recombination rates. Such a task overwhelms our experimental capabilities, but we expect our results would trigger activity in this field.

The temperature dependence of the emission spectra also appears to speak for an extremely poor thermalization of photogenerated carriers in the a-Si NPs. Figures S1(a) and S1(b) of the Supplemental Material [70] show PL spectra of the sample annealed at 550 °C and 700 °C, respectively, measured at different temperatures in the range from 80 to 300 K. The spectra were analyzed using the same line-shape fitting procedure with four Gaussian functions mentioned above, where the peak widths were kept constant at their room-temperature value (this is justified when linewidths are assumed to be dominated by inhomogeneous broadening). The shown spectra were normalized to their maximum intensity for the sake of clarity. Very strikingly, the overall PL intensity only increased by a factor of 5 or 3 for the sample annealed at 550 °C and 700 °C, respectively, when going from room temperature to 80 K. More importantly, there is almost no change in line shape as the temperature is reduced. This behavior, which is an experimental fact independent of any fitting procedure, is certainly at odds with the idea of having a thermal equilibrium occupation of confined states in the a-Si NPs. Such a little effect of temperature on the PL band is in better agreement with a description of the emission by considering significant contributions of hot luminescence from excited states.

Concerning the light-emitting efficiency of the a-Si NPs, a rough but useful estimate is obtained by considering the total number of emitted photons per particle and second divided by the total number of photons per second *absorbed* by each NP from the incident laser beam focused onto the sample. For that purpose, we have taken into account the geometry, the thickness and average refractive index of the oxide layer, the numerical aperture of the collection optics, the NP densities listed in Table I, a mean NP diameter of 2 nm, the incident light power, and the integrated intensity of the whole emission calculated from the measured PL spectra. A crucial ingredient is the magnitude of the absorption coefficient at the laser wavelength, for it has been shown that for the small-NP diameters of our experiments, its value might be more than one order of magnitude lower than for bulk Si [16,71–73]. Due to the lack of information, we decided to use the value of 3×10^3 cm^{-1} for a photon energy of 3 eV reported in Ref. [72] for microporous silicon, which constitutes an upper bound for the absorption coefficient of our a-Si NPs. In this way, we estimate a fair conversion efficiency of 4% for the broadband emission of the particles produced by annealing at 550 °C. For the samples annealed at higher temperature (625 °C and 700 °C), the efficiency diminishes to about 1%, whereas the smaller NPs formed at 450 °C are 10 times less efficient. We notice that the quantum efficiencies extracted here are much lower than the values reported elsewhere [15] for crystalline

NPs, although the amorphous material is supposed to be more efficient due to structural disorder [39]. We believe that the poor figure of merit we obtained is just an indication that only a fraction of the a-Si NPs embedded in the suboxide matrix are optically active. Unsaturated dangling bonds in the amorphous particles, for instance, would rapidly introduce strongly localized states in the gap, which would certainly quench any light emission for that particle.

In order to investigate why the usually strong luminescence from defect centers in the suboxide matrix appears to be almost completely absent in our samples, we have performed a very illustrative experiment: We have illuminated with a strong blue laser (the 488-nm line with a power density of about 2.5 kW/cm^2) the as-grown as well as the Si NP samples for hours. Figure 4 shows the PL spectra measured for the as-grown layer and two samples annealed at 550 °C and 700 °C before and after intense illumination in vacuum. Then, if the samples were kept in vacuum, after about one hour of uninterrupted illumination, the incipient emission band observed in the spectrum of the as-grown sample in Fig. 3(a) grows continuously and immensely in intensity up to the point of becoming the dominant peak. In all three cases, this band centered at around 2.2 to 2.3 eV shoots up in intensity upon light irradiation. In contrast, the PL band associated with the Si NPs remains unaltered by the additional light. We remark that such effect is not observed at ambient conditions. Furthermore, if the chamber where the samples are kept is flooded with air, the defect luminescence disappears immediately, but recovers if the chamber is evacuated and the sample illuminated again. On the contrary, letting pure nitrogen into the chamber has no effect at all on the defect PL. We thus conclude that the presence of molecular oxygen inside the highly porous suboxide matrix is causing the quenching of the defect emission. Strong light frees the O_2 molecules anchored inside the porous matrix, which then diffuse out into the evacuated space. This phenomenology is in accordance with the recently predicted existence of a charge state of the O_2 molecule in oxidized silicon at approximately 1.1 eV above the bottom of the conduction band of Si [74]. Photogenerated electrons might become trapped in these levels, preventing occurrence of any radiative recombination at the defect centers of the suboxide matrix. Moreover, a closely related effect has been observed in cathodoluminescence (CL) measurements on Ge^+, Si^+, and O^+ implanted SiO_2 layers on Si [75]. Electron irradiation during the CL experiments appeared to release atomic or molecular oxygen from defect centers in the alumina, producing "mobile" oxygen which led to destruction of blue/green emitting centers. Finally, we remark that this illumination-induced PL band is the only one which exhibits a clear dependence on environmental conditions and it is observed also in samples not containing Si NPs. On the one hand, this is a proof of its direct relation to the luminescent defect centers of the matrix. On the other hand, the concomitant emission process does not require the presence of Si NPs.

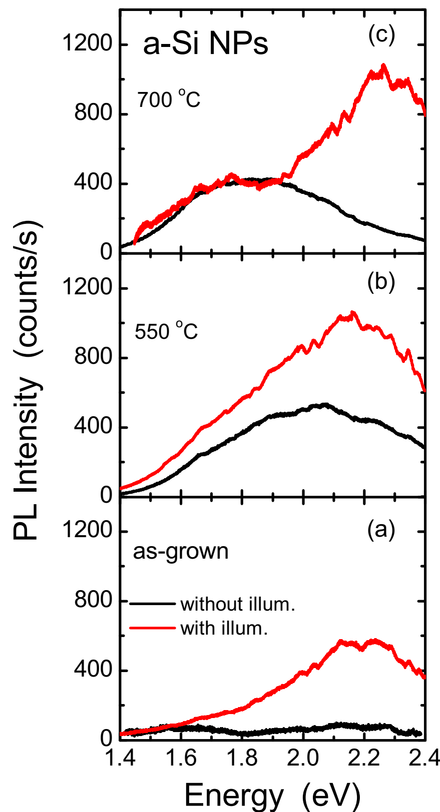

FIG. 4. (Color online) (a) In vacuum and under strong illumination with a blue laser (488-nm line with a power density of about 2.5 kW/cm^2), the incipient PL emission of the as-grown sample transforms into a broad band centered at around 2.2 to 2.3 eV, that grows continuously in intensity becoming the dominant peak. (b), (c) Idem (a) for the samples annealed at 550 °C and 700 °C, respectively. In all three cases, it is the same emission band that appears upon light irradiation. This emission disappears again by breaking the vacuum letting air (O_2) into the sample chamber.

C. PL measurements under pressure

The effect of high hydrostatic pressure on the PL emission of the a-Si NPs is not really pronounced, as displayed by the spectra of Figs. 5(a) and 5(b) measured at three different pressures for the sample annealed at 550 °C and 700 °C, respectively. The width of the Gaussian functions used to fit the PL spectra is much larger that the pressure-induced shift of the peak position. Thus, for a successful fit procedure to account for the line-shape changes with pressure, we had to keep the widths fixed at their ambient pressure values. In fact, since the Gaussian peaks are inhomogeneously broadened, we do not expect any dependence of the widths with pressure. The results for the peak positions of the three lower-energy Gaussians are plotted as a function of pressure for both samples in Fig. 5(c). A first important result is the fact that the pressure coefficient of all three optical transitions is negative and a few meV/GPa in magnitude, close to the corresponding value of the indirect Γ-X gap of bulk Si [55] (see Table II). This provides clear evidence that the confined electron states of the a-Si NPs pick up their main contribution from bulk silicon states with wave vectors within a reciprocal-space region close to the $X_1(\Delta_1)$ conduction-band minimum. The slopes obtained from linear fits to the data points are listed in Table II, together with the pressure coefficients of bulk Si (amorphous and crystalline) and closely related materials such as porous Si. We notice that the linear red-shift of the PL peaks sets in only above 2

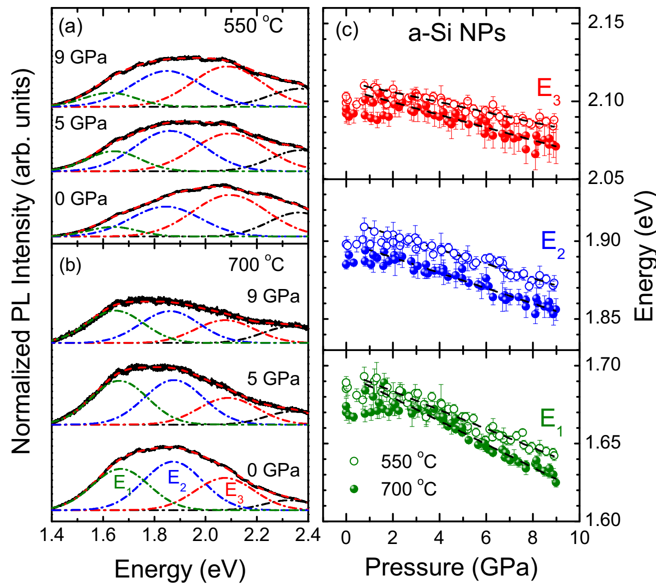

FIG. 5. (Color online) (a) PL spectra of the sample annealed at 550 °C measured at different hydrostatic pressures up to 9 GPa. High pressure causes a small but detectable red-shift of the emission band of the Si NCs. (b) Idem (a) for the sample annealed at 700 °C. (c) The maximum peak position of the three lowest-energy Gaussians as a function of pressure, showing a decreasing linear dependence above 2 to 3 GPa. All data points corresponding to several subsequent pressure upstrokes and downstrokes are shown. The slopes exhibit a striking systematics upon variations in crystal size and depending on the energy of the optical transition.

to 3 GPa, before which the emission bands remain unaltered in their energy position. This behavior is the combined result of the high porosity of the amorphous suboxide matrix and the use of alcohol as pressure-transmitting medium. It appears that pressure is not transmitted to the NPs before the medium has completely infiltrated the suboxide matrix. In fact, when the pressure cell is loaded with liquid He, the emission of the Si NPs shifts to the red immediately upon application of pressure at essentially the same rates, within experimental uncertainty, as with alcohol (see listed coefficients in Table II and Supplemental Material [70]). Exactly the same behavior was observed previously for porous Si depending on the use of alcohol or He as pressure medium [53]. Finally, we note that the energy position as well as the intensity of the $E_1, \ldots, E_3$ peaks are completely reversible upon changes in pressure, except for the very first upstroke due to the sluggish infiltration of the oxide matrix by the pressure medium.

We now compare, on the one hand, our results with those obtained in the pioneering work of Cheong *et al.* on Si nanocrystals in SiO_2 [54], produced by implantation of Si^+ ions into thermally oxidized Si and subsequent annealing at 1100 °C. On the other hand, we also consider the very recent report of Hannah *et al.* on the pressure dependence of the PL from colloidal Si nanoparticles [56]. In the former case, the emission spectrum of the high-density ensemble of Si nanocrystals with average diameter of 3 nm is characterized by a single peak centered at around 1.6 eV with a FWHM of about 200 meV. This peak corresponds well to the ground-state emission in our a-NPs (E_1 peak). The PL measurements were performed at room temperature but using He as pressure medium. The linear pressure coefficients determined in that work and listed in Table II are totally similar to our results. Unfortunately, the use of an oversimplified model for quantum confinement misled the authors in their argumentation, concluding that confinement effects can not explain the difference in excess of a factor 2 between the pressure coefficient of their Si nanocrystals and that of the indirect Γ-X gap of bulk c-Si. Also, for the colloidal Si NPs, a negative but somewhat stronger pressure dependence of the PL maximum position has been

TABLE II. Linear pressure coefficients of the peak-energy position of the three lowest-energy Gaussian functions (E_1, E_2, and E_3) used for the line-shape fits to the PL spectra of two a-Si NP samples. For comparison, we also list the pressure derivative of the main emission band (E^{PL}_{max}) or the indirect band-gap energy (E_{gap}) determined for other nanocrystals (c-Si NPs), crystalline as well as amorphous bulk Si, porous Si, and siloxene. Numbers in parentheses represent error bars. The used pressure-transmitting medium and the pressure range spanned by the linear fit are also indicated.

			Pressure coefficient (meV/GPa)			
Material system	Pressure medium	Pressure range	E_1	E_2	E_3	E^{PL}_{max}/E_{gap}
a-Si NPs (550 °C)	Alcohol	3–9 GPa	−5.8(4)	−4.6(5)	−3.2(5)	
a-Si NPs (700 °C)	Alcohol	2–9 GPa	−7.6(4)	−5.1(4)	−4.1(5)	
	He	0–9 GPa	−8.1(4)	−5.4(4)	−5.1(5)	
c-Si NPs (Ref. [54])	He	0–5 GPa				−4(2)
						−6(2)
c-Si NPs (Ref. [56])	Hexane	0–15 GPa				−17.2
		0–10 GPa				−14.2
		0–15 GPa				−21.3
Porous Si (Ref. [53])	He	0–5 GPa				−13(2)
	Alcohol	3–6 GPa				−20(2)
c-Si bulk (Ref. [76])	Alcohol	0–11 GPa				−14.1(6)
c-Si bulk (Ref. [55])	He	0–8 GPa				−14.5(2)
a-Si bulk (Ref. [77])	Alcohol	0–7.5 GPa				−20(5)
Siloxene (Ref. [78])	Xe	0–5 GPa				−24(3)

determined [56] (see Table II). We point out that the reason for the larger absolute values of the pressure coefficients reported in Ref. [56] most probably lies in the fact that the authors fitted a linear function to all data points in the whole pressure range of their experiments up to about 15 GPa. In contrast, a linear fit for pressures below 5 GPa would certainly yield less negative slopes in good agreement with the coefficients we have determined. Nevertheless, Hannah *et al.*, as well as we do, take this result as compelling evidence that the PL emission arises from quantum confined states of the Si inclusions. The most striking result of our work, however, is the observation of a systematics in the magnitude of the pressure coefficient of the PL peaks, depending on particle size and emission energy (see Table II). For both samples containing Si NPs with different average size, the magnitude of the linear pressure coefficient decreases (becomes less negative) for recombination processes between higher excited states. Furthermore, the coefficient of the emission peaks E_1 to E_3 for the sample with bigger particles (annealed at 700 °C) are systematically larger than the corresponding ones of smaller NPs (550 °C sample). In the next section, based on results of *ab initio* band-structure calculations, we will provide a tentative explanation for such a remarkable trend in terms of quantum confinement effects.

D. *Ab initio* electronic-structure calculations

We have calculated from first principles the electronic structure and its volume dependence of stand-alone, nanometer-size Si crystals. The calculations have been performed within density functional theory (DFT) as implemented in the SIESTA code [79,80], using norm-conserving pseudopotentials [81], an optimized double-ζ polarized basis set [82], and the generalized gradient approximation (GGA) [83]. The nanocrystals are constructed by placing Si atoms at the sites of a diamond structure with the lattice parameter previously obtained for bulk silicon within a sphere of diameter d. Dangling bonds at the surface were passivated by hydrogen termination. Nanocrystal diameters ranging from 1 to 4 nm were considered. Since external pressure is an ill-defined magnitude for a stand-alone crystal, the bond contraction versus applied hydrostatic pressure was first mapped in bulk Si and then such contractions were applied to the nanocrystals to account for an effective pressure. The atomic s and p character of the electronic states is calculated by separately projecting the total density of states on the atomic s and p orbitals.

At this stage, we should justify why the conclusions obtained from calculations performed for perfect nanometer-size crystals should also apply for amorphous particles. First of all, it has been shown that for the correct description of the NP electronic levels it is vital to start from a high-quality structure model of bulk a-Si [51]. This means that the proposed amorphous structure should possess a radial distribution function in agreement with the experimental one and that the electronic density of states (DOS) should yield a well-defined gap without levels within the gap (otherwise, such a nanoparticle would be dark). Unfortunately, this is out of our actual capabilities. Second, it is completely unknown how to apply pressure to an amorphous cluster without explicitly accounting for the embedding oxide matrix. In addition, its compressibility also depends on the particular model structure being used. Nevertheless, it has been argued and demonstrated that for an amorphous material exhibiting an electronic structure still composed of valence and conduction bands separated by a gap but with band tails of disorder-induced localized states, the boundary conditions imposed by the finite size of the NP have very similar effects on the extended states as for c-Si clusters [50]. Tight-binding calculations performed for a-Si NPs with diameters smaller than 2.5 nm have strikingly shown that the most localized states disappear and the remaining states (close to the gap or not) exhibit full confinement, suggesting that for this size range the origin of PL emission is direct band-to-band recombination [50,51].

Hence, we first checked that the pressure dependence of the fundamental band gaps of bulk c-Si is well accounted for within our computational framework. For the lowest direct $\Gamma_{15} - \Gamma_{25'}$ and indirect $X_1(\Delta_1) - \Gamma_{25'}$ gaps we obtained a linear coefficient of $+7$ and -19 meV/GPa, respectively, being the latter in fairly good agreement with the available experimental values listed in Table II. The states corresponding to the top of the valence band as well as both conduction band minima Γ_{15} and $X_1(\Delta_1)$ have predominantly atomic p-type character. For the $\Gamma_{2'} - \Gamma_{25'}$ gap, in contrast, we calculated a coefficient of $+130$ meV/GPa. This is the lowest *direct* gap in Ge and most of zinc-blende III-V and II-VI semiconductor compounds but in Si the $\Gamma_{2'}$ conduction band minimum is pushed up in energy due to the huge bonding-antibonding splitting of the atomic s-type levels, which are by far more sensitive to a reduction of lattice parameter than p-type orbitals [84]. For instance, the pressure coefficients of this direct gap for Ge, GaAs, and ZnSe are 121 meV/GPa, 108 meV/GPa, and 79 meV/GPa, respectively [52].

As an example, the nanocrystal constructed with a diameter of 3 nm is depicted in Fig. 6(a). The resulting density of states with energies up to about 1 eV from the top of the valence band and the bottom of the conduction band is shown in Fig. 6(a). The DOS curve is smooth because a line broadening of 50 meV was artificially introduced for each calculated eigenvalue to ease the comparison with the experiment. We note that the eigenvalues appear to bunch together at certain discrete energies, forming the quantized levels of the Si NPs. This leads to a DOS which exhibits peaks with linewidths between 100 to 150 meV, as the ones marked with dashed lines for the conduction band in Fig. 6(a). The Gaussian functions used for the analysis of the PL line shapes certainly resemble these peaks in the DOS, being energy differences as well as widths in fair agreement between theory and experiment.

To simulate the effect of an externally applied pressure, the electronic-structure calculations were performed at three different lattice parameters corresponding to the values given by the pressure-volume equation of state of bulk silicon for $P = 0$, 1, and 2 GPa. The linear pressure coefficient of the energy of the conduction band eigenvalues referred to the top of the valence band (E_{TVB}) has been obtained by computing the finite differences at the three selected pressures. The results obtained for six different particle diameters from 1.5 to 4 nm are plotted in Fig. 6(b) as a function of the transition energy relative to the top of the valence band for the lowest quantized electronic levels within 1 eV from the bottom of the conduction band. In this way, we simultaneously account for the expectedly small but not negligible shift of the valence band

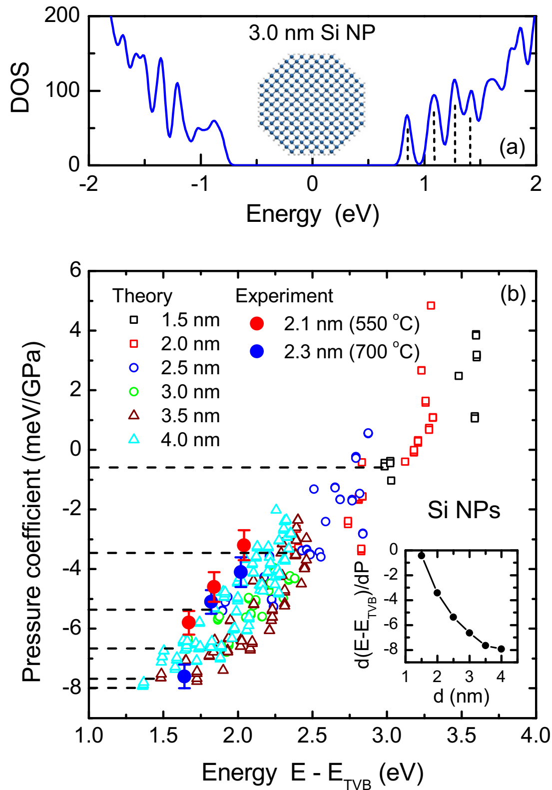

FIG. 6. (Color online) (a) Valence and conduction band density of states (DOS) calculated for the depicted Si nanocrystal with a diameter of 3 nm (solid curve). Peaks corresponding to discrete states were artificially broadened to simulate inhomogeneous broadening in the ensemble, leading to a smooth DOS with peaklike features like the ones marked with dashed vertical lines for the conduction band. (b) The calculated linear pressure coefficients of conduction band eigenvalues referred to the top of the valence band for six different crystal sizes between 1.5 and 4 nm (open symbols). Closed symbols with error bars represent the measured values of the pressure coefficient for transition energies E_1, E_2, and E_3. The inset shows how the calculated pressure coefficient of the conduction band ground state becomes more negative with increasing diameter, reaching eventually the value given by the pressure derivative of the lowest indirect band gap in bulk Si.

under pressure and avoid the introduction of a reference energy when comparing pressure coefficients for different sizes. We note that sign and absolute value of the computed pressure derivatives agree very well with the measured ones (blue and red full symbols with error bars). The most important finding is that both experimental trends regarding the pressure coefficients, which are less negative either for higher excited states of the same NP or for smaller-sized particles, are totally corroborated by the *ab initio* calculations. In addition, it is extremely appealing that all calculated data points appear to crowd and fall on top of a single, universal curve which depends solely on confinement energy. In other words, nearly degenerate confined states will exhibit a similar dependence on pressure, irrespective of the level being the ground state of a smaller particle or the excited state of a larger one. Finally, in the inset to Fig. 6(b), we have plotted the calculated pressure coefficient of the electronic ground-state energy relative to the top of the valence band as a function of diameter. The data points display a tendency to level out for the value of the pressure coefficient of the indirect Γ-X gap of bulk Si (see Table II), in good correspondence with the loss of importance of confinement effects for larger-sized nanoparticles.

The finite size of a system imposes an additional discretization of the electron wave vector up to the point where it loses its status as good quantum number, certainly at the nanometer scale, where translational invariance extends only to a few unit cells. With decreasing size, the Brillouin zone (BZ) folds gradually into its center [85]. This folding is complete for an amorphous material and its energy spectrum is to a good approximation given by the density of states of the band dispersion of the bulk crystal. The wave function of the quantized states in NPs can be always thought as linear combination of bulk band states [86]. Which are the bulk states contributing the most to form the confined-state wave function depends mainly on the energy of the latter. The bulk states with similar energies would span more or less extended wave-vector regions around certain critical points of the electronic band structure. For silicon, the absolute minimum of its conduction band corresponds to the six equivalent valleys at the $X_1(\Delta_1)$ points. Hence, the smaller the crystal or the more excited the energy level, the larger is the confinement energy and the corresponding regions spanned in reciprocal space would lie further inside the BZ and away from the X points. The lowest conduction band of Si has mainly atomic p character (in the Γ–X direction), which explains the small absolute values of the pressure coefficients. The key point, though, is that the deformation potential associated to these p-band states is also wave vector dependent. Close to the Γ_{15} point, the conduction band states exhibit a small but *positive* pressure coefficient, whereas states in the vicinity of the $X_1(\Delta_1)$ point are characterized by a small and *negative* pressure derivative. Hence, the observed systematics for the pressure coefficients is a direct consequence of the reciprocal space folding due to quantum confinement effects: States with higher quantization energies either due to stronger confinement in smaller particles or by being a higher excited level of a larger NP would pick up less negative or even positive contributions to their pressure coefficient from band states with smaller wave vectors further away from the BZ edge at the $X_1(\Delta_1)$ points. Finally, we remark that, in such small amorphous particles, optical transitions occur without the need of being assisted by phonons, thus becoming fairly intense [51]. The wave vectors, well defined only for bulk states of the crystal, are just tags that allow us to sort out the different contributions to the measured effective deformation potential of confined states in the Si NPs.

IV. CONCLUSIONS

In summary, we reported on amorphous Si nanoparticles which exhibit broadband light emission at room temperature and without spurious signal from luminescent defect centers of the surrounding silicon oxide matrix. By making explicit use of high pressures, experimentally as well as theoretically, we were able to shed light on the microscopic origin of such visible emission. Heuristically, the broad emission band appears to be composed of several overlapping PL peaks. Here, we presented experimental evidence and arguments

that allow us to tentatively interpret the peaks in the energy range from 1.5 to 2.2 eV as inhomogeneously broadened optical transitions between quantum confined states (ground as well as excited states) of the a-Si NPs. In particular, the observed size dependence of the linear pressure coefficients of the different PL peaks composing the broad emission band provides strong support to this idea. As shown by the *ab initio* calculations, the sign and magnitude of the pressure derivative of the transition energies from different confined electron states are solely determined by the confinement energy of the latter. With increasing confinement energy, the Si bulk states contributing the most to the confined-level wave function stem from regions in reciprocal space that are further away from the $X_1(\Delta_1)$ point, thus being characterized by less negative or even positive deformation potentials. This settles the quantum confinement model as the correct physical framework to understand the extraordinary improvement in optical properties of amorphous or crystalline nanometer-size silicon inclusions, despite the notorious poor performance of the bulk materials. From the practical point of view, we believe that our strongly luminescent a-Si NPs constitute an interesting alternative to their crystalline counterparts for silicon-based optoelectronics mainly because of the particular preparation method which employs very moderate annealing temperatures and is compatible with CMOS technology.

ACKNOWLEDGMENTS

Special thanks are due to F. J. Belarre for the sample preparation for TEM measurements and the CCiT-UB for the use of the TEM facilities. This work was supported by Spanish Ministry of Science and Innovation (MICINN) through Grants No. CSD2010-00044 (Consolider NANOTHERM), No. CSD2009-00013 (Consolider IMAGINE), No. FIS2012-37549-C05-05, No. MAT2009-09480, No. MAT2010-15138, and No. MAT2010-15202, co-financed by FEDER funds, as well as by Generalitat de Catalunya (Grants No. SGR2009-770, No. SGR2009-1225, and No. XaRMAE). L.R.M. acknowledges support from a JAE fellowship from CSIC co-financed by the European Social Fund.

[1] L. T. Canham, Appl. Phys. Lett. **57**, 1046 (1990).
[2] H. Takagi, H. Ogawa, Y. Yamazaki, A. Ishizaki, and T. Nakagiri, Appl. Phys. Lett. **56**, 2379 (1990).
[3] *Silicon Nanocrystals: Fundamentals, Synthesis and Applications*, edited by L. Pavesi and R. Turan (Wiley-VCH, Weinheim, 2010).
[4] L. Pavesi, L. Dal Negro, C. Mazzoleni, G. Franzo, and F. Priolo, Nature (London) **408**, 440 (2000).
[5] N. Daldosso and L. Pavesi, Laser Photon. Rev. **3**, 508 (2009).
[6] A. G. Cullis and L. T. Canham, Nature (London) **353**, 335 (1991).
[7] W. L. Wilson, P. F. Szajowski, and L. E. Brus, Science **262**, 1242 (1993).
[8] P. Mutti, G. Ghislotti, S. Bertoni, L. Bonoldi, G. F. Cerofolini, L. Meda, E. Grilli, and M. Guzzi, Appl. Phys. Lett. **66**, 851 (1995).
[9] J. P. Wilcoxon, G. A. Samara, and P. N. Provencio, Phys. Rev. B **60**, 2704 (1999).
[10] G. Ledoux, O. Guillois, D. Porterat, C. Reynaud, F. Huisken, B. Kohn, and V. Paillard, Phys. Rev. B **62**, 15942 (2000).
[11] F. Iacona, G. Franzò, and C. Spinella, J. Appl. Phys. **87**, 1295 (2000).
[12] G. Ledoux, J. Gong, F. Huisken, O. Guillois, and C. Reynaud, Appl. Phys. Lett. **80**, 4834 (2002).
[13] M. Zacharias, J. Heitmann, R. Scholz, U. Kahler, M. Schmidt, and J. Bläsing, Appl. Phys. Lett. **80**, 661 (2002).
[14] O. Jambois, H. Rinnert, X. Devaux, and M. Vergnat, J. Appl. Phys. **100**, 123504 (2006).
[15] C. Meier, A. Gondorf, S. Lüttjohann, A. Lorke, and H. Wiggers, J. Appl. Phys. **101**, 103112 (2007).
[16] M. I. Alonso, I. C. Marcus, M. Garriga, A. R. Goñi, J. Jedrzejewski, and I. Balberg, Phys. Rev. B **82**, 045302 (2010).
[17] X. X. Wang, J. G. Zhang, L. Ding, B. W. Cheng, W. K. Ge, J. Z. Yu, and Q. M. Wang, Phys. Rev. B **72**, 195313 (2005).
[18] H. Rinnert, O. Jambois, and M. Vergnat, J. Appl. Phys. **106**, 023501 (2009).
[19] G. G. Qin and Y. Q. Jia, Solid State Commun. **86**, 559 (1993).
[20] A. J. Kontkiewicz, A. M. Kontkiewicz, J. Siejka, S. Sen, G. Nowak, A. M. Hoff, P. Sakthivel, K. Ahmed, P. Mukherjee, S. Witanachchi, and J. Lagowski, Appl. Phys. Lett. **65**, 1436 (1994).
[21] K. S. Min, K. V. Shcheglov, C. M. Yang, H. A. Atwater, M. L. Brongersma, and A. Polman, Appl. Phys. Lett. **69**, 2033 (1996).
[22] S. Gardelis, A. G. Nassiopoulou, M. Mahdouani, R. Bourguiga, and S. Jaziri, Phys. E (Amsterdam) **41**, 986 (2009).
[23] S. M. Prokes and O. J. Glembocki, Phys. Rev. B **49**, 2238 (1994).
[24] L. Tsybeskov, J. V. Vandyshev, and P. M. Fauchet, Phys. Rev. B **49**, R7821 (1994).
[25] Y. Kanemitsu, Phys. Rev. B **49**, R16845 (1994).
[26] L. N. Dinh, L. L. Chase, M. Balooch, W. J. Siekhaus, and F. Wooten, Phys. Rev. B **54**, 5029 (1996).
[27] M. V. Wolkin, J. Jorne, P. M. Fauchet, G. Allan, and C. Delerue, Phys. Rev. Lett. **82**, 197 (1999).
[28] B. Garrido, M. López, O. González, A. Pérez-Rodríguez, J. R. Morante, and C. Bonafos, Appl. Phys. Lett. **77**, 3143 (2000).
[29] A. Sa'ar, Y. Reichman, M. Dovrat, D. Krapf, J. Jedrzejewski, and I. Balberg, Nano Lett. **5**, 2443 (2005).
[30] G. G. Qin and Y. J. Li, Phys. Rev. B **68**, 085309 (2003).
[31] S. Godefroo, M. Hayne, M. Jivanescu, A. Stesmans, M. Zacharias, O. I. Lebedev, G. van Tendeloo, and V. V. Moshchalkov, Nat. Nanotechnol. **3**, 174 (2008).
[32] G. G. Qin, G. Z. Ran, K. Sun, and H. J. Xu, J. Nanosci. Nanotechnol. **10**, 1584 (2010).
[33] W. D. A. M. de Boer, D. Timmerman, K. Dohnalová, I. N. Yassievich, H. Zhang, W. J. Buma, and T. Gregorkiewicz, Nat. Nanotechnol. **5**, 878 (2010).

[34] E. Bustarret, M. Ligeon, and L. Ortéga, Solid State Commun. **83**, 461 (1992).
[35] D. J. Lockwood, Z. H. Lu, and J.-M. Baribeau, Phys. Rev. Lett. **76**, 539 (1996).
[36] K. Murayama, T. Toyama, S. Miyazaki, and M. Hirose, Solid State Commun. **104**, 119 (1997).
[37] R. B. Wehrspohn, J.-N. Chazalviel, F. Ozanam, and I. Solomon, Phys. Rev. Lett. **77**, 1885 (1996).
[38] R. B. Wehrspohn, J.-N. Chazalviel, F. Ozanam, and I. Solomon, Eur. Phys. J. B **8**, 179 (1999).
[39] N.-M. Park, C.-J. Choi, T.-Y. Seong, and S.-J. Park, Phys. Rev. Lett. **86**, 1355 (2001).
[40] B. Delley and E. F. Steigmeier, Phys. Rev. B **47**, 1397 (1993).
[41] Y. Kanemitsu, S. Okamoto, M. Otobe, and S. Oda, Phys. Rev. B **55**, R7375 (1997).
[42] T. Y. Kim, N. M. Park, K. H. Kim, G. Y. Sung, Y. W. Ok, T. Y. Seong, and C. J. Choi, Appl. Phys. Lett. **85**, 5355 (2004).
[43] C. Delerue, G. Allan, and M. Lannoo, Phys. Rev. B **48**, 11024 (1993).
[44] S. Öğüt, J. R. Chelikowsky, and S. G. Louie, Phys. Rev. Lett. **79**, 1770 (1997).
[45] C. S. Garoufalis, A. D. Zdetsis, and S. Grimme, Phys. Rev. Lett. **87**, 276402 (2001).
[46] V. A. Belyakov, V. A. Burdov, R. Lockwood, and A. Meldrum, Adv. Opt. Technol. **2008**, 279502 (2008).
[47] F. A. Reboredo, A. Franceschetti, and A. Zunger, Phys. Rev. B **61**, 13073 (2000).
[48] M. J. Estes and G. Moddel, Appl. Phys. Lett. **68**, 1814 (1996).
[49] D. J. Dunstan and F. Boulitrop, Phys. Rev. B **30**, 5945 (1984).
[50] G. Allan, C. Delerue, and M. Lannoo, Phys. Rev. Lett. **78**, 3161 (1997).
[51] K. Nishio, J. Koga, T. Yamaguchi, and F. Yonezawa, Phys. Rev. B **67**, 195304 (2003).
[52] A. R. Goñi and K. Syassen, Semicond. Semimetals **54**, 247 (1998), and references therein.
[53] H. M. Cheong, P. Wickboldt, D. Pang, J. H. Chen, and W. Paul, Phys. Rev. B **52**, R11577 (1995).
[54] H. M. Cheong, W. Paul, S. P. Withrow, J. G. Zhu, J. D. Budai, C. W. White, and D. M. Hembree, Jr., Appl. Phys. Lett. **68**, 87 (1996).
[55] Z. X. Liu, A. R. Goñi, C. Manz, K. Syassen, K. Brunner, and K. Eberl, Phys. Status Solidi B **219**, 103 (2000).
[56] D. C. Hannah, J. Yang, P. Podsiadlo, M. K. Y. Chan, A. Demortière, D. J. Gosztola, V. B. Prakapenka, G. C. Schatz, U. Kortshagen, and R. D. Schaller, Nano Lett. **12**, 4200 (2012).
[57] P. Pellegrino, B. Garrido, C. Garcia, J. Arbiol, J. R. Morante, M. Melchiorri, N. Daldosso, L. Pavesi, E. Scheid, and G. Sarrabayrouse, J. Appl. Phys. **97**, 074312 (2005).
[58] P. Pellegrino, B. Garrido, J. Arbiol, C. Garcia, Y. Lebour, and J. R. Morante, Appl. Phys. Lett. **88**, 121915 (2006).
[59] H. K. Mao, J. Xu, and P. M. Bell, J. Geophys. Res. **91**, 4673 (1986).
[60] D. M. Zhigunov, V. N. Seminogov, V. Yu. Timoshenko, V. I. Sokolov, V. N. Glebov, A. M. Malyutin, N. E. Maslova, O. A. Shalygina, S. A. Dyakov, A. S. Akhmanov, V. Ya. Panchenko, and P. K. Kashkarov, Physica E (Amsterdam) **41**, 1006 (2009).
[61] C. J. Fang, K. J. Gruntz, L. Ley, M. Cardona, F. J. Demond, G. Müller, and S. Kalbitzer, J. Non-Cryst. Solids **35 and 36**, 255 (1980).
[62] G. Lucovsky, J. Yang, S. S. Chao, J. E. Tyler, and W. Czubatyj, Phys. Rev. B **28**, 3225 (1983).
[63] J. S. Reparaz, A. R. Goñi, M. I. Alonso, M. N. Pérez-Paz, and M. C. Tamargo, Phys. Status Solidi B **244**, 397 (2007).
[64] R. Guerra, F. Cigarini, and S. Ossicini, J. Appl. Phys. **113**, 143505 (2013).
[65] H. Benisty, C. M. Sotomayor-Torres, and C. Weisbuch, Phys. Rev. B **44**, 10945 (1991).
[66] A. N. Poddubny, A. A. Prokofiev, and I. N. Yassievich, Appl. Phys. Lett. **97**, 231116 (2010); **102**, 169903(E) (2013).
[67] A. Pandey and P. Guyot-Sionnest, Science **322**, 929 (2008).
[68] S. V. Kilina, D. S. Kilin, and O. V. Prezhdo, ACS Nano **3**, 93 (2009).
[69] S. V. Kilina, A. J. Neukirch, B. F. Habenicht, D. S. Kilin, and O. V. Prezhdo, Phys. Rev. Lett. **110**, 180404 (2013).
[70] See Supplemental Material at http://link.aps.org/supplemental/10.1103/PhysRevB.89.045428 for a discussion of the temperature dependence of the PL emission of the a-Si NPs in the temperature range between 300 and 80 K and on the influence of the pressure-transmitting medium and the suboxide matrix for the determination of the linear pressure coefficients of the measured optical transitions.
[71] L.-W. Wang and A. Zunger, Phys. Rev. Lett. **73**, 1039 (1994).
[72] D. Kovalev, H. Heckler, G. Polisski, and F. Koch, Phys. Status Solidi B **215**, 871 (1999).
[73] L. Ding, T. P. Chen, Y. Liu, C. Y. Ng, Y. C. Liu, and S. Fung, Appl. Phys. Lett. **87**, 121903 (2005).
[74] A. Alkauskas, P. Broqvist, and A. Pasquarello, Phys. Rev. B **78**, 161305(R) (2008).
[75] H.-J. Fitting, T. Barfels, A. N. Trukhin, B. Schmidt, A. Gulans, and A. von Czarnowski, J. Non-Cryst. Solids **303**, 218 (2002).
[76] B. Welber, C. K. Kim, M. Cardona, and S. Rodríguez, Solid State Commun. **17**, 1021 (1975).
[77] B. A. Weinstein, Phys. Rev. B **23**, 787 (1981).
[78] S. Ernst, M. Rosenbauer, U. Schwarz, P. Déak, K. Syassen, M. Stutzmann, and M. Cardona, Phys. Rev. B **49**, 5362 (1994).
[79] J. M. Soler, E. Artacho, J. D. Gale, A. García, J. Junquera, P. Ordejón, and D. Sánchez-Portal, J. Phys.: Condens. Matter **14**, 2745 (2002).
[80] P. Ordejón, E. Artacho, and J. M. Soler, Phys. Rev. B **53**, R10441 (1996).
[81] N. Troullier and J. L. Martins, Phys. Rev. B **43**, 1993 (1991).
[82] E. Anglada, J. M. Soler, J. Junquera, and E. Artacho, Phys. Rev. B **66**, 205101 (2002).
[83] J. P. Perdew, K. Burke, and M. Ernzerhof, Phys. Rev. Lett. **77**, 3865 (1996).
[84] P. Y. Yu and M. Cardona, *Fundamentals of Semiconductors* (Springer, Berlin, 1995).
[85] A. A. Prokofiev, A. S. Moskalenko, I. N. Yassievich, W. D. A. M. de Boer, D. Timmerman, H. Zhang, W. J. Buma, and T. Gregorkiewicz, JETP Lett. **90**, 758 (2009).
[86] P. Hapala, K. Kusová, I. Pelant, and P. Jelínek, Phys. Rev. B **87**, 195420 (2013).